Disturbance/Uncertainty Estimator Based Robust Control of Nonminimum Phase Systems

Burak Kürkçü, Coşku Kasnakoğlu, and Mehmet Önder Efe

***Abstract*—An open problem in disturbance/uncertainty estimator based control is to obtain explicit mathematical expressions for robust stability, performance, and bandwidth requirement. This paper offers a path based on $\mathcal{H}_\infty$ robust control to resolve this problem. Robust stability/performance is assured at the design phase. The main controller and disturbance observer are handled as a whole. The ideas are applicable to nonminimum phase systems as well. The theory is verified experimentally on a pan–tilt system and numerically on a rotary mechanical system. Comparisons with state-of-the art methods in literature show noticeable performance and robustness improvements.**

***Index Terms*—$\mathcal{H}_\infty$ control, nonminimum phase, pan–tilt, robust stability/performance, rotary mechanical.**

I. Introduction

ROBUSTNESS, disturbance rejection, and performance are prime issues in engineering system design. Advances in science and technology have continuously increased the demand for faster and tougher systems. Control system theory was also influenced by these advances and the evergrowing requirements. In late 1970s, it was revealed that the stability margins of the classical linear quadratic Gaussian design approach are quite poor [1], so the loop transfer recovery (LTR) process was proposed as a remedy [2], [3]. However, robustness properties of the LTR were also seen to suffer in cases such as nonminimum phase systems [4], so the $\mathcal{H}_\infty$ optimization approach was introduced, which has useful properties for nonminimum phase systems [5]. Since then, this approach has undergone various improvements [6]. These studies demonstrated that the problem of robust design for systems having bounded uncertainties can be solved.

The design methods mentioned above have some algebraic and analytical constraints that limit the achievable performance and robustness specifications on the control system design [7]. These constraints include the number of right half-plane (RHP) zeros, uncertainties and unmodeled dynamics, which collectively make it hard or impossible to satisfy arbitrary design requirements. In addition, typically only limited information is available about disturbances and uncertainties. Many design methodologies have been proposed to handle these problems that can be classified into two main groups. The first group is a wide class of linear/nonlinear design approaches that do not require an additional disturbance/uncertainty estimation. The aim is to improve the sensitivity of the control system in order to reduce the effect of disturbances and uncertainties while the system remains robustly stable. Examples include constrained adaptive robust control [8], optimized adaptive motion control [9], adaptive backstepping control [10], and sliding mode control [11]. The second group comprises of control system design based on disturbance estimation. These approaches are usually based on inversion methods and utilize prior knowledge about disturbances to achieve rejection [12]–[16]. While these methods provide good estimation and rejection properties for disturbances and uncertainties, they are mostly limited to specific classes of plants with no guaranteed margins for closed-loop stability.

The way that the disturbances enter a system is also an important factor. Many well established control methods have good robustness against matched disturbances but not against unmatched disturbances. Unfortunately, there exist many practical systems where the disturbances do not enter the system through the same channels as the control inputs [17]. Such unmatched cases have been studied using various strategies, such as the estimator-based attitude stabilization control [18] and robust output tracking control [19]. Disturbance observer based control (DOBC) is another common strategy, where the goal is to predict and cancel disturbances and uncertainties with a specially designed estimator [20].While DOBC methods have been gaining significant momentum, recent review works suggest that robust stability, robust performance, and bandwidth related issues still remain as open problems [21].

In the present study, a disturbance/uncertainty estimator (D/UE) based $\mathcal{H}_\infty$ control design for single-input-single-output (SISO) systems is carried out while attempting to shed light on some of the issues including the minimum bandwidth requirement for a given level of uncertainty and the maximum bandwidth requirement due to the presence of RHP zeros. A $\mathcal{H}_\infty$ control strategy is employed, which is applicable also to nonminimum phase systems, a common design limitation that

Manuscript received January 30, 2018; accepted May 6, 2018. Date of publication May 11, 2018; date of current version August 14, 2018. Recommended by Technical Editor L. Wu. This work was supported by the Scientific and Technological Research Council of Turkey (TÜBİTAK) under Project 116E187. *(Corresponding author: Coşku Kasnakoğlu.)*

B. Kürkçü is with the ASELSAN, Inc., Ankara 06172, Turkey, and also with TOBB University of Economics and Technology, Ankara 06510, Turkey (e-mail: bkurkcu@etu.edu.tr).

C. Kasnakoğlu is with TOBB Economics and Technology University, Ankara 06510, Turkey (e-mail: kasnakoglu@etu.edu.tr).

M. Ö. Efe is with Hacettepe University, Ankara 06100, Turkey (e-mail: onderefe@hacettepe.edu.tr).

Color versions of one or more of the figures in this paper are available online at http://ieeexplore.ieee.org.

Digital Object Identifier 10.1109/TMECH.2018.2835658

is often present in industrial systems. One specific example considered is a high precision nonminimum phase pan–tilt system, which is modeled through system identification and controlled with the proposed method. Physical experiments on the system confirm that the response in terms of line-of-sight (LOS) stabilization precision is considerably improved by using a D/UE. A rotary mechanical system is considered as an additional simulation example with similar positive results.

It should be noted that method proposed in this paper bears some structural similarities to disturbance rejection control (DRC) [22]. A DRC is one state-of-the-art method that handles nonminimum phase systems with the design of optimal disturbance observers. This approach is very useful and has numerous important benefits (e.g., the ability to handle time-delay systems) but diverges from the present study in the following:

1) Robust stability is only verified numerically after the design and cannot be established *a priori* as part of the design process.
2) Robust stability is analyzed only considering the disturbance observer and not the main controller.
3) Robust performance and bandwidth requirements are not studied.

The approach proposed in this paper addresses these issues explicitly.

The main contributions of this study can be summarized as follows: Derivation of explicit expressions for robust stability, performance, and bandwidth requirements of the control system, construction of $\mathcal{H}_\infty$ controllers (for both the main loop and the disturbance observer) that are effective on nonminimum phase plants, introduction of the concept of total equivalent disturbance (TED), construction a novel robustness weight, experimental verification of the proposed approach on a nonminimum phase industrial pan–tilt system, and simulation study of a nonminimum phase rotary mechanical system.

The major contribution of this paper compared to [23] is that the current study provides frequency-based shaping of the estimator's working range and performance, as well as deriving the bandwidth limitation and analytical robust stability condition. Difference compared to [12] and [15] are, respectively, the consideration of the robust performance condition and the applicability to nonminimum phase plants. In addition, a new robustness weight $\hat{W}_T$ is introduced for robust stability over all possible plants during the synthesis.

The rest of this paper is organized as follows: Section II proposes the D/UE structure and establishes the underlying theory. Section III outlines the $\mathcal{H}_\infty$ control design approach for the D/UE and the plant. Mathematical expressions for robust stability and performance are derived, and the applicability to nonminimum phase systems is discussed. Section IV presents application results and Section V ends this paper with conclusions and future work ideas.

II. Disturbance/Uncertainty Estimator

A. Background Information

Many classical control design methods are only applicable to systems were disturbances are matched, i.e., are additive to control inputs. Thanks to the notion of equivalent-input-disturbance (EID), however, unmatched-disturbance systems can be transformed to this form under certain assumptions [23], [24]. The EID concept will be utilized as a tool in this paper so it is introduced briefly as follows.

Let an LTI system affected by disturbance $d(t)$ through channel B_d be given as

$$\begin{aligned} \dot{\bar{x}}(t) &= A\bar{x}(t) + Bu(t) + B_d d(t), \quad \bar{x}(0) = x_0 \\ \bar{y}(t) &= C\bar{x}(t) \end{aligned} \tag{1}$$

where $A \in \mathbb{R}^{n\times n}$, $B \in \mathbb{R}^{n\times 1}$, $C \in \mathbb{R}^{1\times n}$, $\bar{x}(t) \in \mathbb{R}^{n\times 1}$, $u(t) \in \mathbb{R}$, $B_d \in \mathbb{R}^{n\times n_d}$, $\bar{y}(t) \in \mathbb{R}$, and $d(t) \in \mathbb{R}^{n_d\times 1}$. Note that the system is stable, strictly proper, and has no feedthrough term, i.e., $D = 0$. We also assume that the system is SISO for the rest of this paper although an extension to the multi-input multioutput (MIMO) case should be possible with some effort. Equation (1) is termed as the mismatch condition for $B \neq B_d$. The EID form can be obtained under the following assumption.

Assumption 1: The system defined by the matrices (A, B, C) is controllable, observable, and has no poles and zeros on the imaginary axis.

Remark 1: Assumption 1 is necessary to guarantee the internal stability of the nominal system and to allow the output of the plant to track a reference input with no steady-state error [25].

An LTI system is said to satisfy the matching condition if disturbances enter the system through its input channels, i.e.,

$$\begin{aligned} \dot{x}(t) &= Ax(t) + B\left(u(t) + d_{ed}(t)\right), \quad x(0) = x_0 \\ y(t) &= Cx(t) \end{aligned} \tag{2}$$

where $x(t) \in \mathbb{R}^{n\times 1}$, $y(t) \in \mathbb{R}$, and $d_{ed}(t) \in \mathbb{R}$ [26].

Definition 1: Let the control input be $u(t) = 0$. For disturbance $d(t)$, the output of system in (1) is $\bar{y}(t)$ and the output of system in (2) is $y(t)$ for disturbance $d_{ed}(t)$. The disturbance $d_{ed}(t)$ is called EID if $\bar{y}(t) = y(t) \quad \forall t \geq 0$.

Lemma 1: If *Assumption 1* is satisfied, there always exists an equivalent input disturbance $d_{ed} \in L_1 \cap L_\infty$ that satisfies *Definition 1* [23].

B. Disturbance/Uncertainty Estimator

In this section, the mathematical model of the proposed estimator for systems represented by equivalent input disturbance and input multiplicative uncertainty is presented. The proposed control system includes two unity-feedback loops. The first one, which includes controller K, is the main loop designed to stabilize the perturbed plant $\hat{P}$ under the unknown disturbance. The goal of the second loop is to estimate the disturbance and uncertainties, where the estimate is obtained at $\hat{u}$. For this purpose, the output of the perturbed system (y_r) and the control input (u_{tot}) are utilized. A block diagram representation of the proposed control system augmented with D/UE is shown in Fig. 1, where K_{obs} is the D/UE controller, $\varepsilon(t) \in \mathbb{R}$ is the error for D/UE, and $u(t) \in \mathbb{R}$ is the main controller's output. The output of K_{obs}, which is actually the estimated disturbances/uncertainties, is denoted as $\hat{u}(t) \in \mathbb{R}$. The total control input applied to the plant

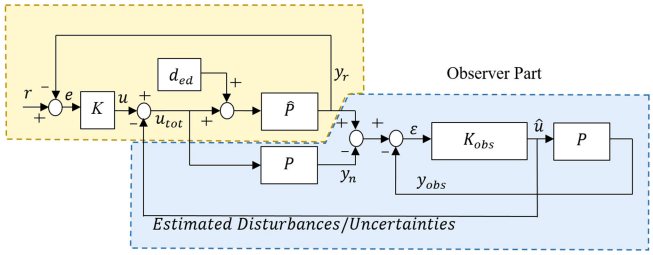

Fig. 1. Overall configuration of the proposed control system.

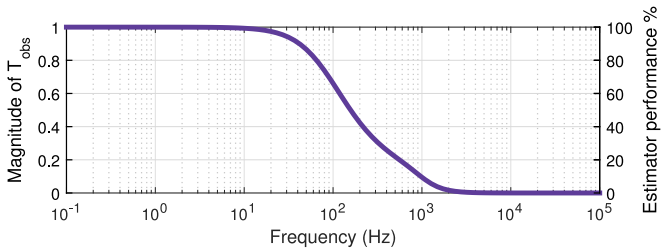

Fig. 2. Basic principle and illustration of estimator performance on a sample complementary sensitivity function.

is $u_{\text{tot}} = u - \hat{u}$, P is the nominal plant (the selected nominal plant), and $\hat{P}$ denotes the perturbed plant (the real plant).

The perturbed plant $\hat{P}$ is defined as

$$\hat{P} \in \{P(1 + \Delta W_T) \quad | \quad \forall \, \|\Delta\|_\infty \leq 1\} \tag{3}$$

where W_T is a robustness weight function and Δ is any stable unstructured uncertainty function. The function W_T must be stable and strictly proper. A generic way to describe the robustness weight function W_T is given in [7] as

$$\left| \frac{M_{ik} e^{j\phi_{ik}}}{M_i e^{j\phi_i}} - 1 \right| \leq |W_T(j\omega_i)| \;\text{ for } i = 1, \ldots, m; k = 1, \ldots, n \tag{4}$$

where the magnitude and the phase are measured at a number of frequencies ω_i (for $i = 1, \ldots, m$) and the experiment is repeated n times based on the application. (M_{ik}, ϕ_{ik}) denotes the magnitude-phase pair measurements for frequency ω_i and experiment k. (M_i, ϕ_i) denotes the magnitude-phase pairs for the nominal plant P. P can also be written as

$$P = C(sI - A)^{-1}B. \tag{5}$$

For the analysis of the D/UE, the nominal plant (P) and the perturbed plant ($\hat{P}$) are considered. The outputs of the perturbed system and the nominal system are, respectively,

$$y_r = \hat{P}(u_{\text{tot}} + d_{ed}), \quad y_n = P u_{\text{tot}}. \tag{6}$$

The application of the $\hat{u}$ on the nominal plant yields the output on the observer loop $y_{\text{obs}}(t) = P\hat{u}$. Then, $\varepsilon(t)$ is defined as

$$y_r - y_n - y_{\text{obs}} = \hat{P}u_{\text{tot}} - P u_{\text{tot}} + \hat{P}d_{\text{ed}} - P\hat{u} := \varepsilon. \tag{7}$$

The design of K_{obs} is possible due to Assumption 1 as a result of which $\varepsilon(t) \to 0$ can be achieved for some desired frequencies. In this study, $\mathcal{H}_\infty$ synthesis is employed for synthesizing K_{obs}, the details of which will be explained in Section III-B. The desired frequency range can be attained by shaping the sensitivity function of observer (S_{obs}), since

$$\varepsilon = (1 + PK_{\text{obs}})^{-1}(y_r - y_n) = S_{\text{obs}}(y_r - y_n). \tag{8}$$

The following lemma deals with what we will call as the *performance* of the estimator.

Lemma 2: The estimation *performance* of the observer can be specified by the complementary sensitivity function of the observer T_{obs} ($T_{\text{obs}} := PK_{\text{obs}}(1 + PK_{\text{obs}})^{-1} = 1 - S_{\text{obs}}$).

Specifically

$$\hat{u} = T_{\text{obs}}(\Delta W_T u_{\text{tot}} + d_{ed} + \Delta W_T d_{ed}). \tag{9}$$

Proof: Using (8) into (7) yields

$$\begin{aligned} P\Delta W_T u_{\text{tot}} + P u_{\text{tot}} - P u_{\text{tot}} + P\Delta W_T d_{ed} \\ + P d_{ed} - P\hat{u} = S_{\text{obs}}(y_r - y_n). \end{aligned} \tag{10}$$

Using (6) in (10) and noting $P \neq 0$ yields

$$\hat{u} = T_{\text{obs}}(\Delta W_T u_{\text{tot}} + d_{ed} + \Delta W_T d_{ed}) \tag{11}$$

which proves (9). ■

There are two useful special cases that follow from the lemma above. If there is no uncertainty (i.e., $\hat{P} = P$), the estimation ($\hat{u}$) is

$$\hat{u} = T_{\text{obs}} d_{ed} \tag{12}$$

and if there is no external disturbance (i.e., $d_{ed} = 0$), it holds that

$$\hat{u} = T_{\text{obs}} \Delta W_T u_{\text{tot}}. \tag{13}$$

The basic principle outlined in Lemma 2 is illustrated in Fig. 2. Absolute magnitude scale is utilized to be able to show the zero point (not possible in decibels) that corresponds to no estimation being made by the D/UE. The transition of T_{obs} from 1 to 0 corresponds to the percentage of disturbances and uncertainties estimated going from 100% to 0% as frequency increases. The estimator works well and estimates all the unknown disturbances and uncertainties in the frequency range where $T_{\text{obs}} \approx 1$. However, if say $|T_{\text{obs}}(j\omega)| = 0.5$ for a given ω, only 50% of the disturbances and uncertainties are estimated. Thus estimation process is highly related with the bandwidth of the D/UE. The problem requirements based on shaping S_{obs} and T_{obs} (and hence the bandwidth) can be achieved by $\mathcal{H}_\infty$ controller design.

The main steps for obtaining the D/UE can be summarized as follows:

1) Generate the control input $u_{\text{tot}} = u - \hat{u}$ and apply it to the selected nominal plant P to get y_n.
2) Generate the reference signal of the D/UE by subtracting y_n from y_r.
3) Design the controller K_{obs} over the nominal plant P so that ε converges to zero for the desired frequencies.

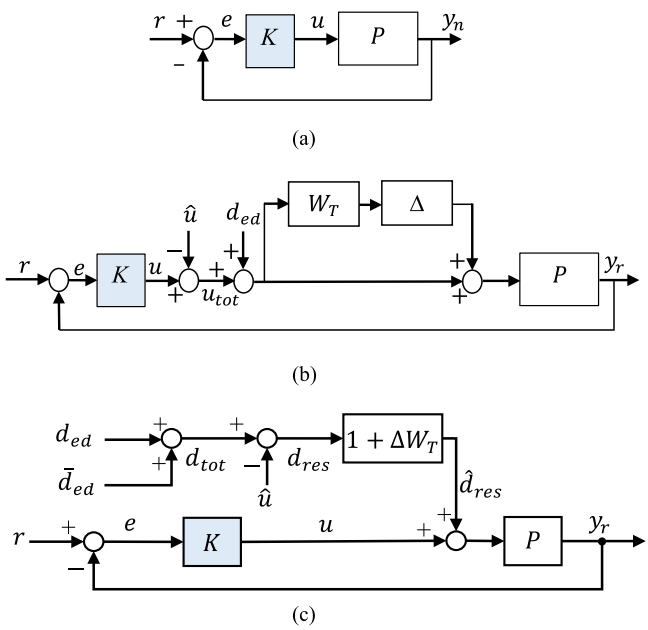

Fig. 3. Block diagrams of the nominal and perturbed systems. (a) Nominal system. (b) Perturbed system. (c) TED form of the perturbed system.

C. Total Equivalent Disturbance

Lemma 2 states that $\hat{u}$ gives an estimation of d_{ed} and on top it some effects that result from the uncertainty ΔW_T (e.g., the terms $T_{\text{obs}}\Delta W_T u_{\text{tot}}$ and $T_{\text{obs}}\Delta W_T d_{ed}$). It is useful for future development to represent all of these effects as a single equivalent disturbance signal.

Definition 2: Fig. 3(a) shows the nominal system P and Fig. 3(b) shows the perturbed system ($\hat{P}$) upon which d_{ed} acts. The *TED* is described as

$$d_{\text{tot}} := \bar{d}_{ed} + d_{ed} \tag{14}$$

where $\bar{d}_{ed}$ is called the *Uncertainty Induced Disturbance (UID)* defined as

$$\bar{d}_{ed} = (1 + \Delta W_T)^{-1}\Delta W_T u. \tag{15}$$

This term represents the effect of the uncertainty ΔW_T excited by the input u seen as an equivalent additive term on the EID d_{ed}. The EID and UID collectively form the TED. The *residual disturbance* d_{res} is defined as the difference between the TED d_{tot} and the estimation $\hat{u}$, i.e.,

$$d_{\text{res}} := d_{\text{tot}} - \hat{u}. \tag{16}$$

Finally, the *perturbed residual disturbance* is

$$\hat{d}_{\text{res}} := (1 + \Delta W_T)d_{\text{res}}. \tag{17}$$

Lemma 3: With Definition 2, the overall system given by Fig. 3(b) is equivalent to the alternative form of the system in Fig. 3(c).

Proof: Fig. 3(b) and (c) becomes equivalent if a given input results in the same output y_r for both cases. For Fig. 3(b)

$$y_r = P(1 + \Delta W_T)(u_{\text{tot}} + d_{ed}). \tag{18}$$

With the help of Definition 2, the output y_r in Fig. 3(c) can be written as

$$y_r = Pu + P\hat{d}_{\text{res}} = Pu + Pd_{\text{res}} + P\Delta W_T d_{\text{res}} \tag{19}$$

expanding and manipulating (19) yields

$$y_r = P(1 + \Delta W_T)(u + d_{ed} - \hat{u})$$

from where (18) follows. ■

By using the TED concept, Lemma 2 can be restructured into the following theorem.

Theorem 1: The estimate produced by the D/UE is

$$\hat{u} = \frac{T_{\text{obs}}(1 + \Delta W_T)}{1 + T_{\text{obs}}\Delta W_T} d_{\text{tot}}. \tag{20}$$

Proof: Substituting u_{tot} with $u - \hat{u}$ in (9)

$$\hat{u} = T_{\text{obs}}(\Delta W_T(u - \hat{u}) + d_{ed} + \Delta W_T d_{ed}).$$

Arranging terms with $\hat{u}$

$$(1 + T_{\text{obs}}\Delta W_T)\hat{u} = T_{\text{obs}}(\Delta W_T u + d_{ed} + \Delta W_T d_{ed})$$

and solving for $\hat{u}$

$$\hat{u} = \frac{T_{obs}(1 + \Delta W_T)}{1 + T_{\text{obs}}\Delta W_T}((1 + \Delta W_T)^{-1}\Delta W_T u + d_{ed}).$$

Using Definition 2

$$\hat{u} = \frac{T_{obs}(1 + \Delta W_T)}{1 + T_{obs}\Delta W_T}(\bar{d}_{ed} + d_{ed}) = \frac{T_{\text{obs}}(1 + \Delta W_T)}{1 + T_{\text{obs}}\Delta W_T} d_{\text{tot}}$$

completes the proof. ■

It is stated by the theorem that the performance of the D/UE is determined by ω_{obs}, which is the bandwidth of the estimator. We define the following terminology:

1) within the BW $\Leftrightarrow T_{\text{obs}} \approx 1 \Leftrightarrow S_{\text{obs}} \approx 0 \Leftrightarrow \omega \ll \omega_{\text{obs}}$;
2) out of the BW $\Leftrightarrow T_{\text{obs}} \approx 0 \Leftrightarrow S_{\text{obs}} \approx 1 \Leftrightarrow \omega \gg \omega_{\text{obs}}$;
3) transition $\Leftrightarrow T_{\text{obs}}, S_{\text{obs}} \not\approx \{0, 1\} \Leftrightarrow \omega$ close to ω_{obs};

based on which the following remarks are useful.

Remark 2: Within the BW, the D/UE makes the perturbed system to behave like the nominal system since TED is perfectly estimated by the D/UE. Investigation of Fig. 3(c) yields that $d_{\text{res}} = d_{\text{tot}} - \hat{u} = 0$, so $\hat{d}_{\text{res}} = (1 + \Delta W_T)d_{\text{res}} = 0$.

Outside the BW, there is no estimation since $T_{\text{obs}} = 0$. Thus, there is no effect of the D/UE ($\hat{u} = 0$) on the perturbed system's behaviour.

Remark 3: The proposed D/UE is also valid for nonminimum phase systems since the estimation process does not contain any direct inversion operation. For such a case however, the design of the D/UE must satisfy some analytical constraints that will be derived in Section III.

III. Controller Design

In this section, $\mathcal{H}_\infty$-controller design based on Linear Fractional Transformation (LFT) framework for the D/UE controller K_{obs} and the main controller K is explained in detail.

A. Background Information and Definitions

We allow the plant to be nonminimum phase as many industrial systems (including the pan–tilt and rotary mechanical

systems to be considered later in this paper) are of this kind. A nonminimum phase plant enforces the following analytical constraint [7], [27]:

$$L_p(z_i) = 0 \tag{21}$$

where $L_p = PK$ is the loop transfer function (LTF) for the nominal system, and $z_i := \mathrm{Re}(z_i) \pm j\mathrm{Im}(z_i)$ denote the RHP zeros of L_p. Also define the RHP zeros for all possible plants $\hat{P}$ as

$$\hat{z} = \left\{ z : \mathrm{Re}(z) > 0 \mid \forall \hat{P} \right\}. \tag{22}$$

Note that this can be an infinite set. This set can be partitioned into the following four subsets:

1) $\hat{z}_1 = \{z : \mathrm{Im}(z) = 0 \mid \forall z \in \hat{z}\}$;
2) $\hat{z}_2 = \{z : \mathrm{Re}(z) \gg \mathrm{Im}(z) \mid \forall z \in \hat{z}\}$;
3) $\hat{z}_3 = \{z : \mathrm{Re}(z) \ll \mathrm{Im}(z) \mid \forall z \in \hat{z}\}$;
4) $\hat{z}_4 = \{z : \mathrm{Re}(z) \approx \mathrm{Im}(z) \mid \forall z \in \hat{z}\}$.

An important task in the design of a control system is to satisfy robust performance objective while the system remains robustly stable. The system satisfies *robust performance condition* if the following two expressions are satisfied at the same time

$$\|W_P \hat{P}\hat{S}\|_\infty < 1 \tag{23}$$

$$\|W_T T\|_\infty < 1 \tag{24}$$

where W_P is the performance weight, $T := PK(1+PK)^{-1}$ is the complementary sensitivity function, $S := (1+PK)^{-1}$ is the sensitivity function, and $\hat{S} := (1+\hat{P}K)^{-1}$ is the sensitivity function for all possible plants. Expression (24) by itself is referred to as the *robust stability criterion* [7]. A possible way to define W_P is given as [27]

$$W_P(s) = \left(\frac{s/\sqrt[k]{M_p} + \omega_b}{s + \omega_b \sqrt[k]{\xi_p}} \right)^k \tag{25}$$

where ω_b is the cutoff frequency for the sensitivity function, M_p is the maximum permissible overshoot for W_P, $\xi_p \ll 1$ to ensure approximate integral action for sensitivity function, and k is an integer greater than 1. For $k = 1$, $M_p = 2$, and $\xi_p = 0$, (21) imposes some bandwidth limitations given as follows [28]:

$$\omega_{b,1} \le |z|/2, \text{ if } z \in \hat{z}_1, \omega_{b,2} \le |z|/4, \text{ if } z \in \hat{z}_2$$

$$\omega_{b,3} \le |z|/2.8, \text{ if } z \in \hat{z}_3, \omega_{b,4} \le |z|, \text{ if } z \in \hat{z}_4$$

where $\omega_{b,i}$ stands for the crossover frequency for an element of the ith subset $(i = 1, 2, 3, 4)$ of $\hat{z}$ and $|z| := \sqrt{\mathrm{Re}(z)^2 + \mathrm{Im}(z)^2}$. Since the subsets can be infinite dimensional, so can the number of crossover frequencies $\omega_{b,i}$. The bandwidth limitation on ω_b in (25) is captured by the following lemma.

Lemma 4: For the perturbed system, the bandwidth limitation on ω_b is

$$\omega_b \le \min\{\omega_{b,1}^+, \omega_{b,2}^+, \omega_{b,3}^+, \omega_{b,4}^+\} \tag{26}$$

where $\omega_{b,1}^+ := \inf\{|\hat{z}_1|\}/2$, $\omega_{b,2}^+ := \inf\{|\hat{z}_2|\}/4$, $\omega_{b,3}^+ := \inf\{|\hat{z}_3|\}/2.8$, $\omega_{b,4}^+ := \inf\{|\hat{z}_4|\}$ and $\inf\{\cdot\}$ denotes the infimum over the corresponding subset.

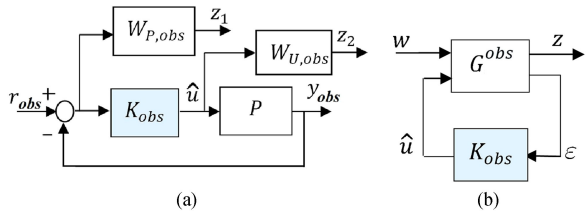

Fig. 4. Block diagrams for synthesis of K_{obs}. (a) D/UE system with weights. (b) LFT framework.

Proof: The magnitude and the phase of the perturbed plant $\hat{P}$ have a bounded deviation, since the form (4) allows only bounded deviations in phase and magnitude. Bode's gain-phase integral relation [27] imposes a direct relation between the phase and the zeros of the plant $\hat{P}$. Thus, the magnitudes of elements of $\hat{z}$ must the bounded from below and since $\hat{z}_1, \hat{z}_2, \hat{z}_3, \hat{z}_4 \subset \hat{z}$, the same bound is valid for the subsets. This implies that the infimum on magnitudes exists for the subsets, which allows for defining

$$\omega_{b,1}^+ := \inf\{|\hat{z}_1|\}/2, \quad \omega_{b,2}^+ := \inf\{|\hat{z}_2|\}/4$$

$$\omega_{b,3}^+ := \inf\{|\hat{z}_3|\}/2.8, \quad \omega_{b,4}^+ := \inf\{|\hat{z}_4|\}. \tag{27}$$

Also define

$$\omega_b^+ := \min\{\omega_{b,1}^+, \omega_{b,2}^+, \omega_{b,3}^+, \omega_{b,4}^+\}. \tag{28}$$

Selecting the bandwidth such that $\omega_b \le \omega_b^+$ makes condition (21) valid for all $\hat{L}_p(z_i)$, which concludes the proof. ■

B. Design Procedure for K_{obs} Using $\mathcal{H}_\infty$ Control

In this section, the design of K_{obs} based on $\mathcal{H}_\infty$ synthesis is explained. The D/UE system can be seen as a weighted nominal system given in Fig. 4(a), which can be transformed into an equivalent LFT version given in Fig. 4(b). Here $W_{P,\mathrm{obs}}$ is the performance weight with the same structure as (25), $W_{U,\mathrm{obs}}$ is the input weighting filter, and G^{obs} is the augmentation of P with these weights. The controller K_{obs} acts only on the nominal plant P, estimating at its output the total disturbance/uncertainty stated by (11). The estimator is effective over a particular band of the frequency spectrum and the estimation of high frequency disturbances or uncertainties are not of interest. To prevent high frequency estimation, the output of K_{obs} is shaped by the weighing function $W_{U,\mathrm{obs}}$. Since the nominal plant P contains RHP zeros, the analytic constraints defined by (21) as well as the bandwidth limitation defined by (26) and (27) are important for $W_{P,\mathrm{obs}}$. The main analytical constraint imposed by a RHP zero is

$$L_{\mathrm{obs}}(z) = 0 \quad \forall z \in \hat{z} \tag{29}$$

where $L_{\mathrm{obs}} = PK_{\mathrm{obs}}$. A general form for the weight $W_{U,\mathrm{obs}}$ is

$$W_{U,\mathrm{obs}}(s) = \left(\frac{s + \omega_u/\sqrt[k]{M_u}}{s\sqrt[k]{\xi_u} + \omega_u} \right)^k \tag{30}$$

where ω_u is the cutoff frequency for $K_{\mathrm{obs}}S_{\mathrm{obs}}$, M_u is the maximum permissible input usage for $K_{\mathrm{obs}}S_{\mathrm{obs}}$, $\xi_u \ll 1$ to prevent

high frequency control input usage, and k is some integer greater than 1.

Define the transfer functions in Fig. 4(b) as

$$\begin{bmatrix} z \\ \varepsilon \end{bmatrix} = \begin{bmatrix} G_{11}^{\text{obs}}(s) & G_{12}^{\text{obs}}(s) \\ G_{21}^{\text{obs}}(s) & G_{22}^{\text{obs}}(s) \end{bmatrix} \begin{bmatrix} w \\ \hat{u} \end{bmatrix} \tag{31}$$

where $z = [z_1 \ z_2]^T$, $w = r_{\text{obs}}$, and $r_{\text{obs}} := y_r(t) - y_n(t)$. The closed-LTF from w to z is given in LFT notation as

$$z = \mathcal{F}_l(G^{\text{obs}}, K_{\text{obs}})w \tag{32}$$

where

$$\begin{aligned} \mathcal{F}_l(G^{\text{obs}}, K_{\text{obs}}) &= G_{11}^{\text{obs}} + G_{12}^{\text{obs}} K_{\text{obs}}(I - G_{22}^{\text{obs}} K_{\text{obs}})^{-1} G_{21}^{\text{obs}} \\ &= \begin{bmatrix} W_{P,\text{obs}} S_{\text{obs}} \\ W_{U,\text{obs}} K_{\text{obs}} S_{\text{obs}} \end{bmatrix} =: N_{\text{obs}}. \end{aligned}$$

The elements of vector z are given by

$$\begin{aligned} z_1 &= W_{P,\text{obs}}\varepsilon = W_{P,\text{obs}}(r_{\text{obs}} - y_{\text{obs}}) \\ &= W_{P,\text{obs}} r_{\text{obs}} - W_{P,\text{obs}} P\hat{u} \\ z_2 &= W_{U,\text{obs}}\hat{u}. \end{aligned} \tag{33}$$

Moreover, the error ε is defined as

$$\varepsilon = r_{\text{obs}} - y_{\text{obs}} = r_{\text{obs}} - P\hat{u}. \tag{34}$$

By using the equations above, the expanded representation of the augmented plant G^{obs} is

$$G^{\text{obs}}(s) = \left[\begin{array}{c:c} W_{P,\text{obs}} & -W_{P,\text{obs}} P \\ 0 & W_{U,\text{obs}} \\ \hdashline 1 & -P \end{array}\right] \tag{35}$$

where $G_{11}^{\text{obs}} = [W_{P,\text{obs}} \ \ 0]^T$, $G_{12}^{\text{obs}} = [-W_{P,\text{obs}} P \ \ W_{U,\text{obs}}]^T$, $G_{21}^{\text{obs}} = 1$, and $G_{22}^{\text{obs}} = -P$. In this notation, the standard $\mathcal{H}_\infty$ control problem is to find a stabilizing controller K_{obs} that minimizes

$$\|\mathcal{F}_l(G^{\text{obs}}, K_{\text{obs}})\|_\infty = \max_\omega \bar{\sigma}(\mathcal{F}_l(G^{\text{obs}}, K_{\text{obs}})(j\omega)) = \gamma_{\text{obs}} \tag{36}$$

where γ_{obs} is the value of $\|\mathcal{F}_l(G^{\text{obs}}, K_{\text{obs}})\|_\infty$ over all stabilizing controllers K_{obs} and $\bar{\sigma}$ denotes the maximum singular value of the given function. The form defined by (36) can be solved iteratively to reach the minimum value of γ_{obs} and the detailed solution can be found in [27] and [28].

C. Robustness Benefits of the D/UE-Based Control System

In this section, important properties and limitations related to robust stability and performance are given for the D/UE-based control system. Recall from Section III-A that the RHP zeros inevitably impose some limitations on the system. However, it can be shown that the augmentation of a D/UE does not cause additional difficulties regarding the RHP zeros. That is, it leaves the analytical constraints unchanged, as captured by the following lemma.

Lemma 5: If the design of K_{obs} satisfies the condition (29) by satisfying (26), then the analytical constraint defined by (21) is unchanged by the augmentation of the D/UE.

Proof: Let $\hat{L}_p$ be the LTF for the perturbed system in Fig. 3(b). From the figure, one can write

$$\begin{aligned} u_{\text{tot}} &= Ke - \hat{u} \\ u_{\text{tot}} &= Ke\frac{1}{1 + T_{\text{obs}}\Delta W_T} - \frac{T_{\text{obs}}(1 + \Delta W_T)}{1 + T_{\text{obs}}\Delta W_T} d_{ed}. \end{aligned} \tag{37}$$

Therefore

$$\begin{aligned} y_r &= \hat{P}(d_{ed} + u_{\text{tot}}) \\ &= \left(1 - \frac{T_{\text{obs}}(1 + \Delta W_T)}{1 + T_{\text{obs}}\Delta W_T}\right)\hat{P}d_{ed} + \hat{P}Ke\frac{1}{1 + T_{\text{obs}}\Delta W_T} \\ &= \frac{S_{\text{obs}}}{1 + T_{\text{obs}}\Delta W_T}\hat{P}d_{ed} + \frac{1}{1 + T_{\text{obs}}\Delta W_T}\hat{P}Ke. \end{aligned} \tag{38}$$

With the help of Fig. 3(b), $\hat{L}_p$ can be defined as the transfer function from error e to the output y_r, i.e.,

$$\begin{aligned} \hat{L}_p &= \frac{\hat{P}K}{1 + T_{\text{obs}}\Delta W_T} \\ &= (P + P\Delta W_T)\frac{K}{1 + T_{\text{obs}}\Delta W_T} \\ &= PK + PK\frac{W_T S_{\text{obs}}}{1 + T_{\text{obs}}\Delta W_T}\Delta. \end{aligned} \tag{39}$$

To avoid unstable pole-zero cancellations, it is required that

$$\hat{L}_p(z) = 0 \quad \forall z \in \hat{z}. \tag{40}$$

As K_{obs} must satisfy (29), i.e., $PK_{\text{obs}}(z) = 0$, this means

$$T_{\text{obs}}(z) = 0 \quad S_{\text{obs}}(z) = 1 \quad \forall z \in \hat{z}. \tag{41}$$

Therefore

$$\hat{L}_p(z) = PK + PKW_T\Delta \quad \forall z \in \hat{z}. \tag{42}$$

The last equation implies that the constraint on $\hat{L}_p$ reduces to the constraint on L_p. Using these derivations

$$\hat{L}_p(z) = 0 \Leftrightarrow L_p(z) = 0 \quad \forall z \in \hat{z}. \tag{43}$$

This concludes the proof. ■

Theorem 2: The robust stability criterion of the proposed system is

$$\left\| W_T T \frac{S_{\text{obs}}}{1 - |W_T T_{\text{obs}}|} \right\|_\infty < 1. \tag{44}$$

Proof: For simplicity, it is assumed that $L_p = PK$ is stable. The closed-loop system in Fig. 3(a) is also stable since Nyquist plot for L_p does not enclose the point $-1 + j0$. The LTF of the overall system is given in (39). If some LTF in the uncertainty set encircles the point $-1 + j0$, then there is another LTF in the same uncertainty set that crosses exactly $-1 + j0$ at some frequency since the set of all possible plants is norm-bounded.

For robust stability, this must be avoided. So

$$\begin{aligned}\text{RS} &\Leftrightarrow |1+\hat{L}_p| \neq 0 \quad \forall\omega \quad \forall\hat{L}_p \\ &\Leftrightarrow |1+\hat{L}_p| > 0 \quad \forall\omega \quad \forall\hat{L}_p \\ &\Leftrightarrow \left|1+PK+PK\frac{W_T S_{\text{obs}}}{1+T_{\text{obs}}\Delta W_T}\Delta\right| > 0 \quad \forall\omega \quad \forall\Delta.\end{aligned} \tag{45}$$

The worst case occurs when $|\Delta| = 1$ and the phases of the terms $1+PK$ and $PK\frac{W_T S_{\text{obs}}}{1+T_{\text{obs}}\Delta W_T}\Delta$ have opposite signs. Thus

$$\begin{aligned}\text{RS} &\Leftrightarrow |1+PK| - \left|PK\frac{W_T S_{\text{obs}}}{1+T_{\text{obs}}\Delta W_T}\right| > 0 \quad \forall\omega \\ &\Leftrightarrow \left|\frac{W_T S_{\text{obs}}}{1+T_{\text{obs}}\Delta W_T}T\right| < 1 \quad \forall\omega.\end{aligned} \tag{46}$$

The following operation is given to simplify previous one:

$$\begin{aligned}1 &= |1+\Delta W_T T_{\text{obs}} - \Delta W_T T_{\text{obs}}| \\ &\leq |1+\Delta W_T T_{\text{obs}}| + |W_T T_{\text{obs}}| \quad \forall\omega.\end{aligned} \tag{47}$$

Using (47) in (46) yields

$$1 - |W_T T_{\text{obs}}| \leq |1+\Delta W_T T_{\text{obs}}| \quad \forall\omega \tag{48}$$

$$\left|\frac{W_T S_{\text{obs}}}{1+T_{\text{obs}}\Delta W_T}\right| \leq \left|\frac{W_T S_{\text{obs}}}{1-|W_T T_{\text{obs}}|}\right| \quad \forall\omega. \tag{49}$$

Using this final expression, it is clear that (46) holds if

$$\left|\frac{W_T S_{\text{obs}}}{1-|W_T T_{\text{obs}}|}T\right| < 1 \quad \forall\omega$$

which is the statement of the theorem.

Remark 4: The stability assumption on L_p in the proof can be removed by requiring that L_p and $\hat{L}_p$ have the same number of RHP-poles. In other words, it must be ensured that the perturbations do not change the number of encirclements occurring in the nominal case. ■

Corollary 1: Let

$$\hat{W}_T := \frac{W_T S_{\text{obs}}}{1-|W_T T_{\text{obs}}|}. \tag{50}$$

This is a valid robustness weight function using which the statement of Theorem 2 can be written as

$$\|\hat{W}_T T\|_\infty < 1. \tag{51}$$

Proof: The requirements for a robustness weight function are stability and strictly properness [27]. $\hat{W}_T$ is such a function since W_T, S_{obs} are stable, strictly proper, and $1-|W_T T_{\text{obs}}|$ is a scalar. Substituting (50) into (44) completes the proof. ■

Theorem 3: The robust performance criteria of the proposed system is

$$\left\|\frac{W_P \hat{P} S S_{\text{obs}}}{1-|W_T T_{\text{obs}}|}\right\|_\infty < 1. \tag{52}$$

Proof: The robust performance goal can be posed as minimizing the effect of the disturbance on the output [27]. The transfer function between d_{tot} to y_r can be written by the help of Fig. 3(a) as follows:

$$y_r = PKe + P(1+W_T\Delta)d_{\text{res}} \tag{53}$$

$$(1+PK)y_r = \hat{P}d_{\text{res}} \tag{54}$$

which leads to the frequency domain transfer function

$$\frac{y_r}{d_{\text{res}}} = \frac{P(1+\Delta W_T)}{1+PK} = \hat{P}S. \tag{55}$$

Expressing in terms of amplitude

$$|y_r| = |\hat{P}S d_{\text{res}}| \tag{56}$$

and using (16)

$$|y_r| = |\hat{P}S(d_{\text{tot}} - \hat{u})|. \tag{57}$$

From Theorem 1

$$|y_r| = \left|\hat{P}S d_{\text{tot}} - \hat{P}S\frac{T_{\text{obs}}(1+\Delta W_T)}{1+T_{\text{obs}}\Delta W_T}d_{\text{tot}}\right| \tag{58}$$

$$|y_r| = \left|\frac{\hat{P}S S_{\text{obs}} d_{\text{tot}}}{1+T_{\text{obs}}\Delta W_T}\right|. \tag{59}$$

Rearranging and weighing with W_P

$$\left|\frac{W_P y_r}{d_{\text{tot}}}\right| = \left|\frac{W_P \hat{P} S S_{\text{obs}}}{1+T_{\text{obs}}\Delta W_T}\right| \tag{60}$$

and requiring the expression to be less than unity for all frequencies imply

$$\left|\frac{W_P \hat{P} S S_{\text{obs}}}{1+T_{\text{obs}}\Delta W_T}(j\omega)\right| < 1 \qquad \forall\omega \quad \forall\Delta. \tag{61}$$

By the help of (47) and (48)

$$\left|\frac{W_P \hat{P} S S_{\text{obs}}}{1-|T_{\text{obs}} W_T|}(j\omega)\right| < 1 \qquad \forall\omega \quad \forall\Delta \tag{62}$$

which is same with (52). ■

As long as $|S_{\text{obs}}| < 1$, Theorem 3 implies that the D/UE helps robust performance by decreasing the left-hand side of (52). Within the bandwidth of the estimator, $S_{\text{obs}} \approx 0$, so the condition holds automatically provided that internal stability exists. This is understandable as the system becomes identical to the nominal system when all the uncertainties and disturbances are cancelled (Remark 2). Outside the bandwidth, $S_{\text{obs}} \approx 1$ and the robust performance condition reduces to the case without the D/UE.

D. $\mathcal{H}_\infty$ Controller Design for K

In this section, the design of the main controller K based on $\mathcal{H}_\infty$ theory is explained. The general scheme for controller synthesis is given in Fig. 5(a) and the LFT version is given in Fig. 5(b). Here, $\hat{W}_T$ is defined by Corollary 1, G is the plant augmented with the weights, and K is the main controller.

The system in Fig. 5(b) can be expressed as

$$\begin{bmatrix} z \\ e \end{bmatrix} = \begin{bmatrix} G_{11}(s) & G_{12}(s) \\ G_{21}(s) & G_{22}(s) \end{bmatrix} \begin{bmatrix} w \\ u \end{bmatrix} \tag{63}$$

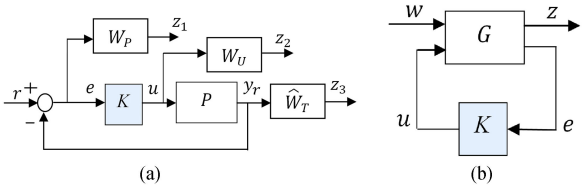

Fig. 5. Block diagrams for synthesis of K. (a) Control loop including K. (b) LFT framework.

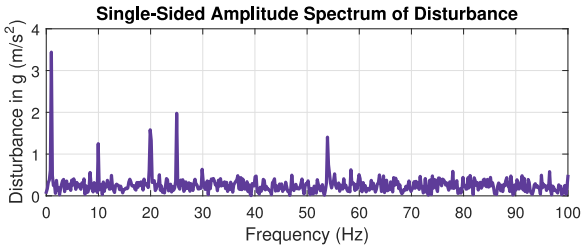

Fig. 6. Amplitude spectrum of the disturbance profile.

where $z = [z_1\ z_2\ z_3]^T$ and $w = r$. The closed-LTF from w to z is given by the LFT

$$z = \mathcal{F}_l(G, K)w \tag{64}$$

where

$$\begin{aligned}\mathcal{F}_l(G,K) &= G_{11} + G_{12}K(I - G_{22}K)^{-1}G_{21} \\ &= \begin{bmatrix} W_P S \\ W_U K S \\ \hat{W}_T T \end{bmatrix} =: N.\end{aligned} \tag{65}$$

The elements of vector z are given by

$$\begin{aligned} z_1 &= W_P e = W_P(r - y_r) = W_P r - W_P P u \\ z_2 &= W_U u \\ z_3 &= \hat{W}_T P u. \end{aligned} \tag{66}$$

The error e is defined as

$$e = r - y_r = r - Pu. \tag{67}$$

By using the equations above, the augmented plant G can be partitioned as

$$G(s) = \left[\begin{array}{c|c} W_P & -W_P P \\ 0 & W_U \\ 0 & \hat{W}_T P \\ \hline 1 & -P \end{array}\right] \tag{68}$$

where $G_{11} = [W_P\ \ 0\ \ 0]^T$, $G_{12} = [-W_P P \quad W_U \quad \hat{W}_T P]^T$, $G_{21} = 1$, and $G_{22} = -P$. The standard $\mathcal{H}_\infty$ control problem is to find a stabilizing controller K that minimizes

$$\|\mathcal{F}_l(G, K)\|_\infty = \max_\omega \bar{\sigma}(\mathcal{F}_l(G, K)(j\omega)) < \gamma \tag{69}$$

where γ is the value of $\|\mathcal{F}_l(G, K)\|_\infty$ over all stabilizing controllers K. The form defined by (69) can be solved iteratively to reach the minimum value of γ and the detailed solution can be found in [27] and [28].

IV. Application Examples

A. Nonminimum Phase High-Precision Pan–Tilt System Control

In this section, experiments based on the proposed control system are done for a high-precision pan–tilt system. This pan–tilt system is an official product of ASELSAN, Inc. The system and experimental environment are shown in Fig. 7(a). The direct drive motors are mounted on the origin of the axes (elevation and azimuth) to provide motion to the pan–tilt system. These motors are controlled by standard motor drivers. The pan–tilt system is utilized in a naval pointing and tracking application. The sensor suit mounted on the system includes a three-axis IMU unit of bandwidth 200 Hz, as well as a day-TV/infrared camera and/or a laser module depending on the application. The pan-axis is rotated continuously at fixed speed to capture a 360° view. The control goal is to keep the camera's LOS fixed despite all the motion, vibration, and disturbances by stabilizing the tilt-axis. The standard industrial measure for the performance of the pan–tilt control system is how much the camera image moves, i.e., the *pixel deflection* of the camera.

At the core of the system is the xPC target that includes the control algorithms, communication channels, A/D, and D/A conversion channels. Inside the xPC target, a Xilinx FPGA chip is used to run the control structure. In digitizing the controllers, bilinear transformation (Tustin method) is used as it yields a good match with continuous-time. Digital stabilization loop is operated at 3 kHz frequency. Rate feedbacks are obtained via the RS422 channel of the xPC target. Corresponding current references that are the outputs of the controllers are sent by D/A channels to the motor drivers. Typically the current controller is tuned for around 1 kHz bandwidth. This is quite high compared to the pan–tilt mechanical bandwidth, so the current LTF can be approximated as a constant. The analog current reference is compared to the actual current and the error enters to an analog PI controller. The result of the PI controller is compared to a triangle signal and the corresponding PWM signals that drive the MOSFETS of power converters are generated. Clamping diodes serve as an antiwindup structure in the analog current loop. The final output is the required current to be supplied to the motors.

The main focus of this example is to design a D/UE-based robust controller to minimize the angular displacement of the tilt-axis subject to external effects and uncertainties. A nominal model of pan–tilt system is obtained through data collection and system identification. Then, weight functions describing the performance and robustness specifications are defined. The $\mathcal{H}_\infty$ control law for the D/UE and perturbed plant are built using MATLAB/Simulink. The controllers are compiled and embedded into the xPC target environment for real-time execution on the experimental hardware. A six degree-of-freedom (6-DoF) Stewart platform is used to supply disturbances for laboratory testing. This platform can generate custom disturbance profiles up to 100 Hz. The pan–tilt system is mounted to the center of the top of the platform and the platform is excited to simulate vibrations that would be encountered on the sea in real-life. Po-

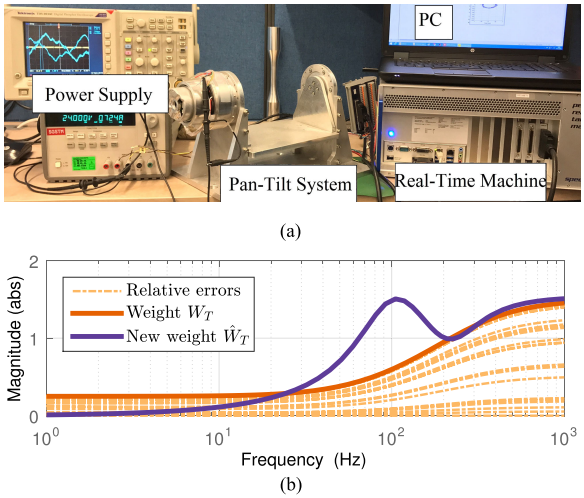

Fig. 7. Experimental setup and its modeling. (a) Pan–tilt system and the real-time target machine. (b) Relative errors for experimental data, a first-order bounding weight W_T, and the new robustness weight $\hat{W}_T$.

tential mechanical disturbance sources include fluid flow, slosh, wave motion, actuator reaction torques, and cryogenic cooler pump disturbances. Any of these may induce jitter into the optical components in a beam path as well as contribute to base motion disturbance. The amplitude spectrum of an excitation scenario is given in Fig. 6. The proposed methodology is also compared to the EID estimator approach in [23] and [24], and to the classical PID control, in order to show the improvement gained by the proposed structure.

The first step is determining the nominal plant with subspace system identification (N4SID) [29], resulting in

$$P = \frac{s-3101}{s+3101}\,\frac{-0.85308(s+3101)}{s^2+369.8s+1057}.$$

The torque command for the motor is selected as the input while the gyro signal is selected as the output for the tilt-axis. The nominal system is a stable and nonminimum phase system since there is a RHP zero, amenable to the method proposed in this study. Time-delay between the IMU unit and the electronic cards is believed to be the main reason for the RHP zero [30]. While system identification based modeling is utilized in this paper, physics-based modeling approaches to pan/tilt systems also support the presence of RHP zeros [31]. The variation of the identified nominal plant is obtained using different pay-loads. In addition to the IMU unit, some applications need a day-TV/infrared-camera and/or a laser module, and the controller needs to work for all pay-loads and in the presence of high-frequency modeling errors. For this purpose, the system identification is carried numerous times for varying conditions, resulting in

$$W_T(s) = (1.5s+399)/(s+1596). \tag{70}$$

Modeling errors, the bounding weight W_T, and the new weight $\hat{W}_T$ are given in Fig. 7(b). The performance requirements for the system are disturbance rejection up to 35 Hz is required, the maximum possible disturbance imposed on system

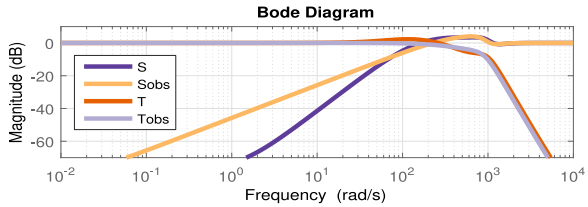

Fig. 8. Sensitivity and complementary sensitivity functions of the nominal system and D/UE.

is 20 dB at 6 Hz, and closed-loop bandwidth requirement is 60 Hz. To meet these requirements, the weights used for designing K_{obs} are

$$W_{P,\text{obs}} = \left(\frac{\frac{s}{1.5}+750}{s+750\times 0.0001}\right) \quad W_{U,\text{obs}} = \left(\frac{\frac{s+6280}{\sqrt[3]{500}}}{s\sqrt[3]{0.0001}+6280}\right)^3$$

from which the design is carried out using the procedure described in Section III-B. The parameter $M_p = 1.5$ means that the maximum overshoot for ε is 1.5 times a given step function at r_{obs}. $M_u = 500$ means that the output/input ratio of the transfer function $K_{\text{obs}}S_{\text{obs}}$ is 500 for a given step error ε at the control input $\hat{u}$. These are worst case limitations on the S_{obs} and $K_{\text{obs}}S_{\text{obs}}$ if $\gamma_{\text{obs}} = 1$. With lower γ_{obs}, the results achieved may be lower. In addition, the frequency-based shaping of $K_{\text{obs}}S_{\text{obs}}$ defines the disturbance/uncertainty rejection range since $\hat{u}$ is directly related to this function. The estimator design was completed with $\gamma_{\text{obs}} = 0.92$, which is close to limit performance where K_{obs} was computed as a seventh-order system. The weights used to design of the main controller K are given as

$$W_P(s) = \left(\frac{s/\sqrt{2}+188}{s+188\sqrt{0.0001}}\right)^2, \; W_U(s) = W_{U,\text{obs}}(s). \tag{71}$$

The design of main controller K was completed with $\gamma = 0.97$, where K was computed as an eleventh-order controller. The corresponding sensitivity/complementary sensitivity functions of D/UE and those of the nominal system are shown in Fig. 8. As seen from T_{obs} and S_{obs}, the D/UE works well up to roughly 100 Hz.

Next, the pan–tilt system is placed on a 6-DoF Stewart platform that oscillates based on a given disturbance profile. As an initial test, the system is excited with sinusoidal test inputs of frequencies 1 and 20 rd/s, respectively. These are all within the estimator's bandwidth so the system behaves identical to the nominal system as shown in Fig. 9. Also shown for comparison is the case when the D/UE is turned OFF.

The robust stability and robust performance conditions as defined by Theorems 2 and 3 are shown in Fig. 10 for the system with and without the D/UE. It is seen that robust performance is achieved with the D/UE but not without it. Also note that outside the observer's bandwidth, its estimation vanishes so the plots for the two cases converge to each other for high frequencies.

The performance for pan–tilt systems in vision applications are typically measured in pixel deflection of the image or the equivalent angular displacement of the axes. It is desirable for the camera image to move no more than one pixel, which

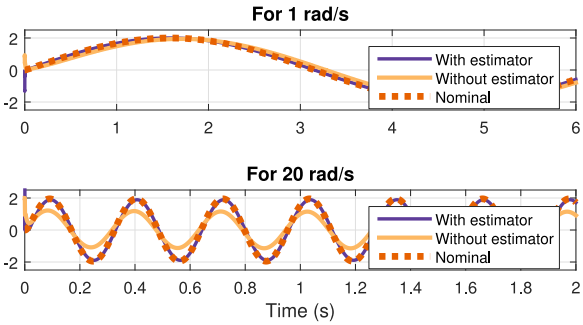

Fig. 9. Outputs of the nominal system and perturbed system for different payloads with/without the D/UE under excitations at various frequencies.

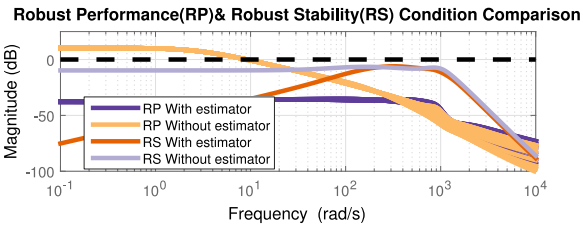

Fig. 10. Comparison of the robust stability/performance criteria with/without the D/UE.

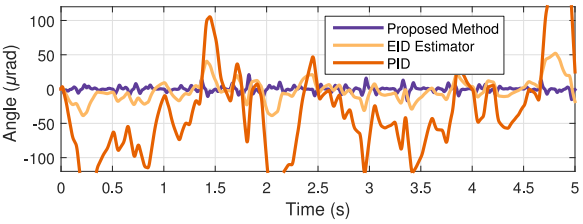

Fig. 11. Comparison of the angular displacement for the proposed method, EID approach, and classical PID.

corresponds to 25 μrd in our application. Fig. 11 shows that with the D/UE, the maximum angular displacement is approximately 20 μrd, which is acceptable. In comparison for the EID approach [23], [24], the angular displacement reaches to about 48 μrd. For the PID controller, the angular displacement takes values as high as 200 μrd. The parameters used to design EID Estimator are given as follows:

$$Q_K = \text{diag}[1\ \ 1\ \ 1\ \ 10], \quad R_K = 1 \times 10^{-4}$$

$$Q_L = \text{diag}[1\ \ 1\ \ 1] \times 10^3, \quad R_L = 1$$

$$[K_P|K_R] = [0.0074\ 0.1724\ 1.1922|3.871] \times 10^4,\ T_F = 0.01\text{s}$$

$$L = [-0.001\ \ 0.0451\ \ 0.0163]^T, \quad K_F = 0.98$$

$$B^+ = [0.7814\ \ 4.5039\ \ 0.0973] \times 10^3, \quad \rho = 10^6.$$

The definitions and explanations of these parameters are found in [23] and [24]. The standard DOBC design such as that in [13] and [15] was not applicable for this problem due to the presence of the RHP zero. As for the PID controller, we have experimented with various manual and automated tuning methods and the best case obtained is the one shown in the figure.

The experimental results seem to support that the outlined approach, in comparison to alternate options, provides improvements in the direction of high closed-loop performance under the presence of noise, uncertainties, and RHP poles.

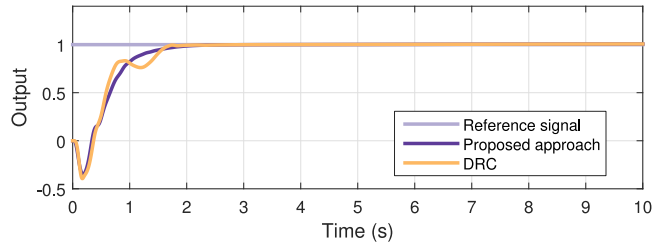

Fig. 12. Step response of the system under constant disturbances.

B. Nonminimum Phase Rotary Mechanical System Control

In this section, a complex rotary mechanical nonminimum phase system is taken as a benchmark to illustrate the effectiveness of the proposed method. The system consists of inertias, dampers, torsional springs, a timing belt, pulleys, and gears. The transfer function of the plant is taken directly from [22] and is given as

$$P(s) = \frac{123.853 \times 10^4 \times (-s + 3.5)}{(s^2 + 6.5s + 42.25)(s + 45)(s + 190)}. \tag{72}$$

The unstable zero at 3.5 is close to the imaginary-axis in contrast to the example in the preceding section. Also, note that the poles -45 and -190 are located far away from the complex conjugate pole pair $-3.2500 \pm 5.6292j$. The defined robustness weight for the system is given as

$$W_T(s) = (0.2s + 3)/9. \tag{73}$$

Since W_T allows a maximum 34% deviation both in magnitude and phase of the plant at 3.5 rd/s, the minimum location of the unstable zero of the system remains unchanged. Moreover, the system has only a real unstable zero. These imply

$$w_b^+ = \min w_{b,1}^+ = \inf\{|\hat{z}_1|\}/2 = 1.75 \text{ rd/s}. \tag{74}$$

From this point on the design is carried out similar to the preceding section following the procedure in Section III. A comparison with the DRC approach [22] is also done under the same parameter values and the same constant disturbance profile as in that work. The result is given in Fig. 12. Although the undershoot characteristics of both methods behave similar, the proposed method removes the undesired transient oscillations when compared to the DRC. For the proposed method, the RS condition defined by (44) was satisfied with 0.9615, meaning that the overall system is guaranteed to remain robustly stable under plant variations and constant disturbances.

V. Conclusion and Future Works

A D/UE-based robust control approach is developed theoretically, after which its prominent performance is demonstrated experimentally on a high-precision nonminimum phase pan–tilt system and numerically on a complex rotary mechanical system. Explicit expressions for robust stability, performance, and bandwidth are derived, which had been proposed as open problems

in recent reviews on DOBC systems. The D/UE augmentation is shown to be applicable without difficulty to nonminimum phase plants since it leaves the analytical constraints for RHP zeros unchanged. Experiments conducted on the pan–tilt setup reveal that the proposed estimator provides significant improvement in precision compared to the case where it is absent, as well alternate methods in literature. Simulation results on a rotary mechanical system in comparison to other state-of-the-art methods also support these statements.

Future research directions include expansion of the theory to MIMO systems, as well as realizations on other industrial experiments.

REFERENCES

[1] J. Doyle, "Guaranteed margins for LQG regulators," *IEEE Trans. Automat. Control*, vol. 23, no. 4, pp. 756–757, Aug. 1978.

[2] J. Doyle and G. Stein, "Robustness with observers," *IEEE Trans. Automat. Control*, vol. 24, no. 4, pp. 607–611, Aug. 1979.

[3] B. Kurkcu and C. Kasnakoglu, "LQG/LTR position control of an BLDC motor with experimental validation," in *Proc. 9th Int. Conf. Elect. Electron. Eng.*, 2015, pp. 796–800.

[4] J. C. Doyle and G. Stein, "Multivariable feedback design: Concepts for a classical/modern synthesis," *IEEE Trans. Automat. Control*, vol. 26, no. 1, pp. 4–16, Feb. 1981.

[5] G. Zames, "Feedback and optimal sensitivity: Model reference transformations, multiplicative seminorms, and approximate inverses," *IEEE Trans. Automat. Control*, vol. 26, no. 2, pp. 301–320, Apr. 1981.

[6] J. C. Doyle, K. Glover, P. P. Khargonekar, and B. A. Francis, "State-space solutions to standard $\mathcal{H}_2$ and $\mathcal{H}_\infty$ control problems," *IEEE Trans. Automat. Control*, vol. 34, no. 8, pp. 831–847, Aug. 1989.

[7] J. C. Doyle, B. A. Francis, and A. R. Tannenbaum, *Feedback Control Theory*. Chelmsford, MA, USA: Courier Corporation, 2013.

[8] W. Sun, H. Gao, and O. Kaynak, "Vibration isolation for active suspensions with performance constraints and actuator saturation," *IEEE/ASME Trans. Mechatronics*, vol. 20, no. 2, pp. 675–683, Apr. 2015.

[9] H.-H. Chiang, K.-C. Hsu, and I.-H. Li, "Optimized adaptive motion control through an SoPC implementation for linear induction motor drives," *IEEE/ASME Trans. Mechatronics*, vol. 20, no. 1, pp. 348–360, Feb. 2015.

[10] W. Sun, H. Gao, and O. Kaynak, "Adaptive backstepping control for active suspension systems with hard constraints," *IEEE/ASME Trans. Mechatronics*, vol. 18, no. 3, pp. 1072–1079, Jun. 2013.

[11] J. Zheng, H. Wang, Z. Man, J. Jin, and M. Fu, "Robust motion control of a linear motor positioner using fast nonsingular terminal sliding mode," *IEEE/ASME Trans. Mechatronics*, vol. 20, no. 4, pp. 1743–1752, Aug. 2015.

[12] K. Khayati, "Multivariable adaptive sliding-mode observer-based control for mechanical systems," *Can. J. Elect. Comput. Eng.*, vol. 38, no. 3, pp. 253–265, 2015.

[13] B. A. Güvenç, L. Güvenç, and S. Karaman, "Robust mimo disturbance observer analysis and design with application to active car steering," *Int. J. Robust Nonlinear Control*, vol. 20, no. 8, pp. 873–891, 2010.

[14] J. Yang, W.-H. Chen, and S. Li, "Non-linear disturbance observer-based robust control for systems with mismatched disturbances/uncertainties," *IET Control Theory Appl.*, vol. 5, no. 18, pp. 2053–2062, 2011.

[15] E. Sarıyıldız and K. Ohnishi, "A guide to design disturbance observer," *J. Dyn. Syst., Meas., Control*, vol. 136, no. 2, 2014, Art. no. 021011.

[16] H. Li, X. Ning, and B. Han, "Composite decoupling control of Gimbal servo system in double-gimbaled variable speed CMG via disturbance observer," *IEEE/ASME Trans. Mechatronics*, vol. 22, no. 1, pp. 312–320, Feb. 2017.

[17] B. Kürkçü and C. Kasnakoğlu, "Estimation of unknown disturbances in Gimbal systems," *Appl. Mech. Mater.*, vol. 789, pp. 951–956, 2015.

[18] B. Xiao, Y. Shen, and O. Kaynak, "Attitude stabilization control of flexible satellites with high accuracy: An estimator-based approach," *IEEE/ASME Trans. Mechatronics*, vol. 22, no. 1, pp. 349–358, Feb. 2017.

[19] S. Su and Y. Lin, "Robust output tracking control for a velocity-sensorless vertical take-off and landing aircraft with input disturbances and unmatched uncertainties," *Int. J. Robust Nonlinear Control*, vol. 23, no. 11, pp. 1198–1213, 2013.

[20] W.-H. Chen, "Disturbance observer based control for nonlinear systems," *IEEE/ASME Trans. Mechatronics*, vol. 9, no. 4, pp. 706–710, Dec. 2004.

[21] W.-H. Chen, J. Yang, L. Guo, and S. Li, "Disturbance-observer-based control and related methods - an overview," *IEEE Trans. Ind. Electron.*, vol. 63, no. 2, pp. 1083–1095, 2016.

[22] L. Wang and J. Su, "Disturbance rejection control for non-minimum phase systems with optimal disturbance observer," *ISA Trans.*, vol. 57, pp. 1–9, 2015.

[23] J.-H. She, X. Xin, and Y. Pan, "Equivalent-input-disturbance approach–analysis and application to disturbance rejection in dual-stage feed drive control system," *IEEE/ASME Trans. Mechatronics*, vol. 16, no. 2, pp. 330–340, Apr. 2011.

[24] R.-J. Liu, M. Wu, G.-P. Liu, J. She, and C. Thomas, "Active disturbance rejection control based on an improved equivalent-input-disturbance approach," *IEEE/ASME Trans. Mechatronics*, vol. 18, no. 4, pp. 1410–1413, Aug. 2013.

[25] W. S. Levine, *The Control Handbook*. Boca Raton, FL, USA: CRC Press, 1996.

[26] J. Yang, S. Li, and W.-H. Chen, "Nonlinear disturbance observer-based control for multi-input multi-output nonlinear systems subject to mismatching condition," *Int. J. Control*, vol. 85, no. 8, pp. 1071–1082, 2012.

[27] K. Zhou and J. C. Doyle, *Essentials of Robust Control*, vol. 104. Upper Saddle River, NJ, USA: Prentice-Hall, 1998.

[28] S. Skogestad and I. Postlethwaite, *Multivariable Feedback Control: Analysis and Design*. Hoboken, NJ, USA: Wiley, 2007.

[29] P. Van Overschee and B. De Moor, "N4SID: Subspace algorithms for the identification of combined deterministic-stochastic systems," *Automatica*, vol. 30, no. 1, pp. 75–93, 1994.

[30] S. Al-Amer and F. Al-Sunni, "Approximation of time-delay systems," in *Proc. Amer. Control Conf.*, 2000, vol. 4, pp. 2491–2495.

[31] Y. Luzanov, "Modeling off-the-shelf pan/tilt cameras for active vision systems," Master thesis, Dept. Comput. Eng., Rochester Inst. Technol., Rochester, NY, USA, May 2006.

Burak Kürkçü received the B.S. degree from the Department of Mechanical Engineering, Istanbul Technical University, Istanbul, Turkey, in 2010, and the M.S. degree from the Department of Electrical and Electronics Engineering, TOBB University of Economics and Technology, Ankara, Turkey, in 2015, where he is currently working toward the Ph.D. degree.

His research interests include dynamical modeling, nonlinear, robust, and adaptive control with applications to aerospace industry.

Coşku Kasnakoğlu received the B.S. degrees from the Department of Electrical and Electronics Engineering and the Department of Computer Engineering, Middle East Technical University, Ankara, Turkey, in 2000, and the M.S. and Ph.D. degrees from the Department of Electrical and Computer Engineering, Ohio State University, Columbus, OH, USA, in 2003 and 2007, respectively.

He is currently a Professor with the Department of Electrical and Electronics Engineering, TOBB University of Economics and Technology, Ankara, Turkey.

Mehmet Önder Efe received the B.S. degree from the Department of Electronics and Communications Engineering, Istanbul Technical University, Istanbul, Turkey, in 1993, the M.S. degree from the Department of Systems and Control Engineering, Boğaziçi University, Istanbul, Turkey, in 1996, and the Ph.D. degree from the Department of Electrical and Electronics Engineering, Boğaziçi University, in 2000.

He is currently the Head of the Department of Computer Engineering, Hacettepe University, Ankara, Turkey.

Dr. Efe is also an Associate Editor for the IEEE TRANSACTIONS ON INDUSTRIAL ELECTRONICS, IEEE TRANSACTIONS ON INDUSTRIAL INFORMATICS, IEEE/ASME TRANSACTIONS ON MECHATRONICS, and *Transactions of the Institute of Measurement and Control.*